University of Seville

Master in Nuclear Physics

Orbit simulations of fast-ion transport induced by externally applied 3D magnetic perturbations in the ASDEX Upgrade tokamak.

Author:

Jesús González Rosa

Supervisors:

Eleonora Viezzer and Manuel García Muñoz

Departamento de Física Atómica, Molecular y Nuclear

Facultad de Física

Plasma Science and Fusion Technology

Centro Nacional de Aceleradores

Abstract

Externally applied 3D magnetic perturbations break the symmetry of the magnetic field in a tokamak and have an impact on the transport of fast-ions, i.e. suprathermal ions. It was shown that the variation of the toroidal canonical momentum gives a measured for the radial transport of fast-ions.

In this thesis, experiments of the ASDEX Upgrade tokamak were analyzed in terms of the radial transport of fast-ions. Simulations using the Monte Carlos orbit-following code ASCOT were carried out in order to study the impact of externally applied 3D magnetic perturbations on the topology of the orbits and to quantify the radial fast-ion transport.

The results show that when the magnetic perturbations are applied a drift appears (changing the trajectory of the particle) and the transport created depends on the initial pitch angle, radius and energy of the particles and the equilibrium. Also, it is confirmed that the strong correlation between fast-ion losses and impurity toroidal rotation is related to the trapped-passing boundary .

Contents

Chapter 1

Introduction

1.1 Thermonuclear fusion

The sun produces energy by nuclear fusion reactions. This energy is transmitted to us via radiation. A huge part of the energy that we use in our everyday life come from fusion in the stars. For this reason, the idea of extracting energy directly from nuclear fusion is very interesting.

The nuclear fusion reaction consists in two light nuclei that are fused into a heavier one. In this process, the energy that allows the nuclei to stay together becomes kinetic energy of the reaction products. In the case of a fusion reactor, two isotopes of hydrogen (deuterium, tritium) and the light isotope of helium (^3He) can be used as fuel. These reactions can be described by the equations [1]:

$$D + D \rightarrow T(1.0\ \text{MeV}) + p(3.0\text{MeV}) \tag{1.1}$$

$$D + D \rightarrow^3 He(0.8\text{MeV}) + n(2.5\text{MeV}) \tag{1.2}$$

$$D + T \rightarrow^4 He(3.5\text{MeV}) + n(14.1\text{MeV}) \tag{1.3}$$

$$D +^3 He \rightarrow^4 He(3.6\text{MeV}) + p(14.7\text{MeV}) \tag{1.4}$$

The reaction with the largest cross section at the temperature of 10 keV (the temperature range achievable in today's experiment) will be the most profitable. As we can see in the Figure 1.1, the DT reaction has the largest cross section, therefore, we will use deuterium and tritium as a fuel.

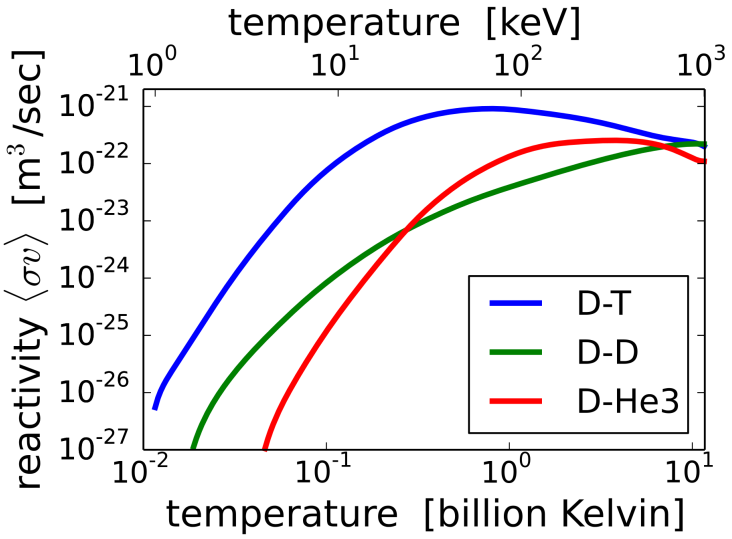

Figure 1.1: Nuclear reaction (1.1)-(1.4) cross sections [2].It is observed the cross section of the reaction between deuterium and tritium (blue), between deuterium and deuterium (green) and deuterium and helium-3 (red).

Deuterium can be extracted from seawater and tritium will be obtained in the reactor from isotopes of lithium that react with the neutrons [3]. The fission reactions are

$$^6Li + n \rightarrow T + ^4He + 4.8\text{MeV} \tag{1.5}$$

$$^7Li + n \rightarrow T + ^4He + n - 2.5\text{MeV} \tag{1.6}$$

where the fast neutrons produce tritium. Furthermore, deuterium and lithium are abundant and well distributed geographically, so there will be no problem to obtain these resources.

Also, the fusion reaction produces isotopes of helium and hydrogen. Helium and most part of hydrogen isotopes are radioactively stable except tritium, however tritium has a short half life of 12.3 years, so it does not require a long term storage.

In the fusion reaction, two nuclei have to collide with enough energy to overcome the Coulomb repulsion. This requires high temperature on the order of a hundred million Kelvin. At this temperature the matter is an ionized gas that it is called plasma.

There are two approaches to plasma confinement: inertial and magnetic confinement.

In inertial confinement, the fusion occurs by high pressure of the fuel, this pressure comes from a rapidly compression of the fuel pellets. In magnetic confinement, the plasma is suspended in vacuum using a magnetic field and heated by electromagnetic waves and

particle beams until a sufficient temperature is reached. In this master thesis, simulations for experiments carried out at a magnetic confinement fusion device with the goal to study the orbits topology generated in this conditions and their relations with the equilibrium and the tranport of fast ion.

1.2 Tokamaks

The most promising method to contain the plasma via magnetic confinment is the tokamak. A tokamak is a toroidal vacuum chamber in which the plasma can be suspended by a magnetic field [3]. The tokamak is a torus device (a surface or solid formed by rotating a closed curve, especially a circle, about a line which lies in the same plane but does not intersect it). In tokamaks, the major radius (the distant between the main axis and the magnetic axis) is larger than the radius of the circle, called the minor radius. We describe this system using cylindrical coordinates (R,z, φ). The plane that is formed by R and z coordinates is the poloidal plane and the direction that is perperdicular to this plane is the toroidal direction, this is observed in the Figure 1.2.

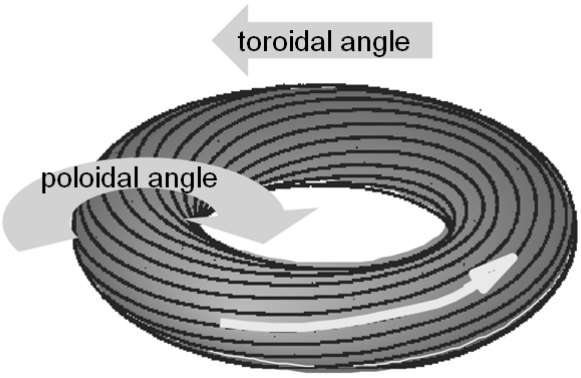

Figure 1.2: Tokamak schematic representation of the magnetic field along the toroidal angle and the poloidal angles.[4]

The field of a tokamak is the superposition of a toroidal field generated by the coils surrounding the vessel and a poloidal field generated by the induction of a toroidal current

in the plasma by a current that flows in a central solenoid. In Figure 1.3 it is observed the magnetic field.

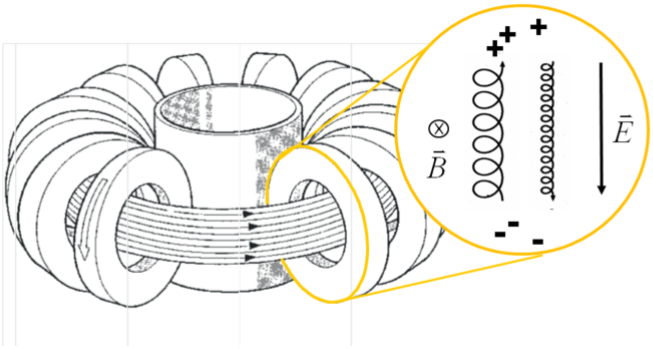

Figure 1.3: Schematic magnetic field of the tokamak [4]. We include a cut of a section of the tokamak where the magnetic field is represented.

This field creates surfaces of constant magnetic flux in the tokamak. These flux surfaces can intersect the wall (open flux surface) or not (closed flux surface). Closed flux surfaces span the core plasma, where fusion can take place. Open flux surfaces form the edge plasma also called Scrape-Off Layer (SOL) region. The plasma can flow along flux surfaces but only the closed flux surfaces are capable of confining the plasma for certain time. The core and the SOL are separated by the last closed flux surface, also known as separatrix (Figure 1.4). The divertor is the area where the open flux surfaces intersect the vessel. The analysis of the data carried out in this thesis is based on experiments carried out in the mid-size tokamak ASDEX Upgrade (located in Garching, Germany) [5].

In theory, when the release of fusion energy compensates for the losses and the reaction becomes selfsustained, the ignition is achieved. The Lawson criterion gives a relation between the peak ion density (n in m^{-3}), temperature (T, in keV) and confinement time (τ_e, in seconds) for ignition to be achieved:

$$n \cdot T \cdot \tau_e > 5 \cdot 10^{21} m^{-3} \cdot keV \cdot s \tag{1.7}$$

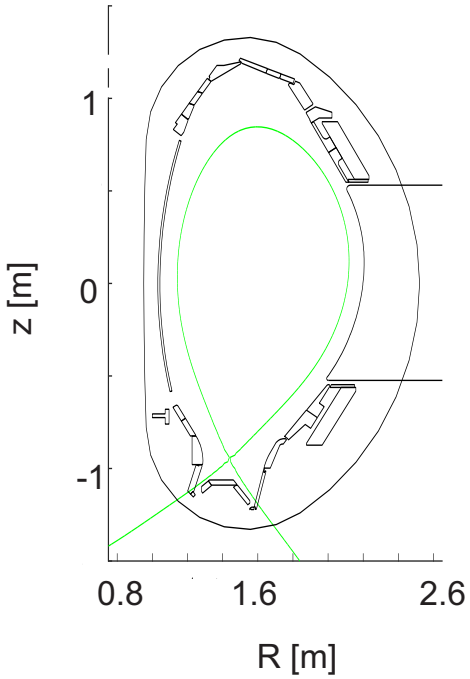

Figure 1.4: Poloidal cross section of the AUG vessel showing the separatrix, is highlighted in green.

1.3 Motivation

The goal of this thesis is to study the variation of the toroidal canonical momentum and its relation with the transport of the fast-ions and the trapped-passing boundary and confirming the impact of the trapped-boundary [5] in the correlations between plasma rotation, plasma density and fast-ions losses.

The transport of the fast-ions depends on the equilibrium and is related to the variation of the toroidal canonical momentum of the particles [6]. The ASCOT Code will be used to scan the initial radius, energy and pitch angle [See 2.1] of different discharges. The variation of the toroidal canonical momentum and the changes of the tranport created by a perturbation of the magnetic field will be analysed and their relations will be confirmed .

It is considered that the correlations between plasma rotation, plasma density and fast-ions losses are related to the orbit topology [5]. In this thesis, the initial radiogyrus and pitch angle [See 2.1] will be scanned using the ASCOT Code to confirm a agreement between the correlations and the trapped-passing boundary.

Chapter 2

Theoretical Background

2.1 Particle motion

Particles in the tokamak are in the presence of a magnetic and electric field. The movement of these particles is described by the Lorentz force [3],

$$m\ddot{\vec{r}} = Ze(\vec{E} + \dot{\vec{r}} \times \vec{B}) \tag{2.1}$$

where m is the mass of the particle, Z is the charge number of the particle, e is the unit charge, $\vec{r}$ is the position of the particle, $\dot{\vec{r}} = v$ is the velocity of the particle, $\ddot{\vec{r}}$ is the acceleration of the particle, $\vec{E}$ is the electric field and $\vec{B}$ is the magnetic field.

In absence of an electric field, the particle turns around the magnetic field lines, this movement is called gyromotion. The radius of this gyration is the Larmor radius,

$$r_L = \frac{mv_\perp}{ZeB} \tag{2.2}$$

where $v_\perp$ is the perpendicular component of the velocity (the parallel component would be $v_\parallel$). It is convenient to separate the gyration of the particle with the trajectory of the guiding centre (the axis of the trajectory of the particle). The trajectory of the guiding centre is subject to drifts (Figure 2.1).

In this thesis, it is necesary the study the pitch angle(Λ) of a particle, it will be an important parameter. Its definition is

$$\Lambda = arccos(\frac{v_\parallel}{v}) \tag{2.3}$$

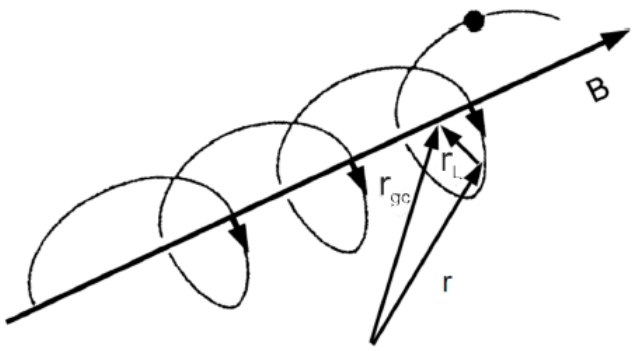

Figure 2.1: Helical orbit of a particle. Decomposition of particle motion in its gyration around the magnetic field and the motion of the guiding centre, where r is the vector position of the particle, r_L is the Larmor radius and r_{gc} the vector position of the guiding centre.

which depends of the inclination of the magnetic field lines.

Drifts are produced by a force that is perpendicular to the magnetic field or by a variation of the magnetic field [7].

The first case is called a curvature drift,

$$\vec{v} = \frac{\vec{F_\perp} \times \vec{B}}{qB^2} \tag{2.4}$$

In this case, the particle tries to follow the field line but feels a centrifugal force. This drift is independent of the charge.

In the second case, the magnetic field can be written as,

$$\vec{B} = \vec{B_0} + (\vec{r} \cdot \nabla)\vec{B} \mid_0 \tag{2.5}$$

The magnetic field does not vary much with the curvature, it is proportional to the inverse of the radius. The expression of the gradient can be written as,

$$\vec{v}_{\nabla B} = \frac{mv^2}{2B^3Ze}(\vec{B} \times \nabla B) \tag{2.6}$$

This drift causes separation of charges and creates an electric field. To prevent this we create a poloidal current that mitigates this effect.

2.1.1 Particle orbits

In a tokamak, the particle orbits are classified in two big groups: trapped (Figure 2.2) and passing orbits (Figure 2.3).

Passing orbits circle the poloidal cross section of the tokamak. In axisymmetric geometry, the passing orbits close on themselves in the poloidal plane.

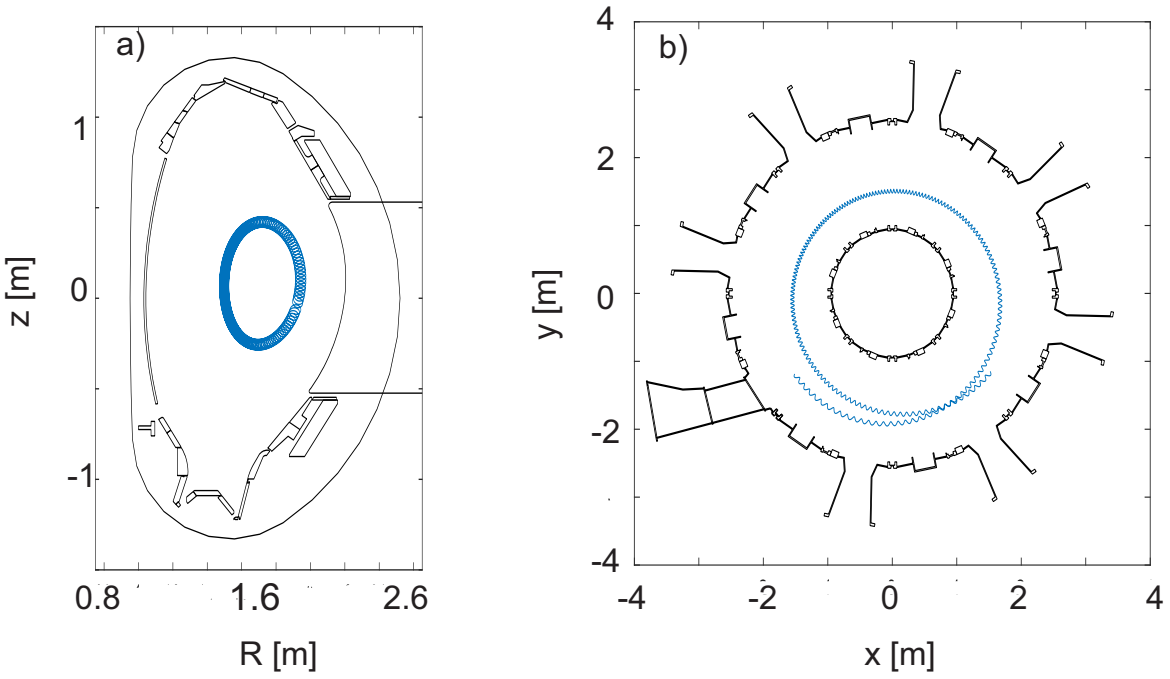

Figure 2.2: Poloidal cross section (a) and toroidal cross section (b) of a passing trajectory.

Particles can be trapped on the low field side of the magnetic field (the field is proportional to the inverse of the radius). The magnetic moment (it is an adiabatic invariant) and the energy are conserved. The expression of the magnetic moment is,

$$\mu = \frac{m v_\perp^2}{2B} \tag{2.7}$$

When the particle moves to higher field the perpendicular component of the velocity must increase to conserve the magnetic moment, for this reason the parallel component of the velocity must decrease to conserve the energy. If we reach $v_\parallel = 0$, the parallel acceleration proportional to $-\nabla B$ reflects the particle towards the low field side. This type of orbits is referred to as banana or trapped orbits.

We cross the trapped-passing boundary when the particles begin to describe trapped trajectories instead of passing.

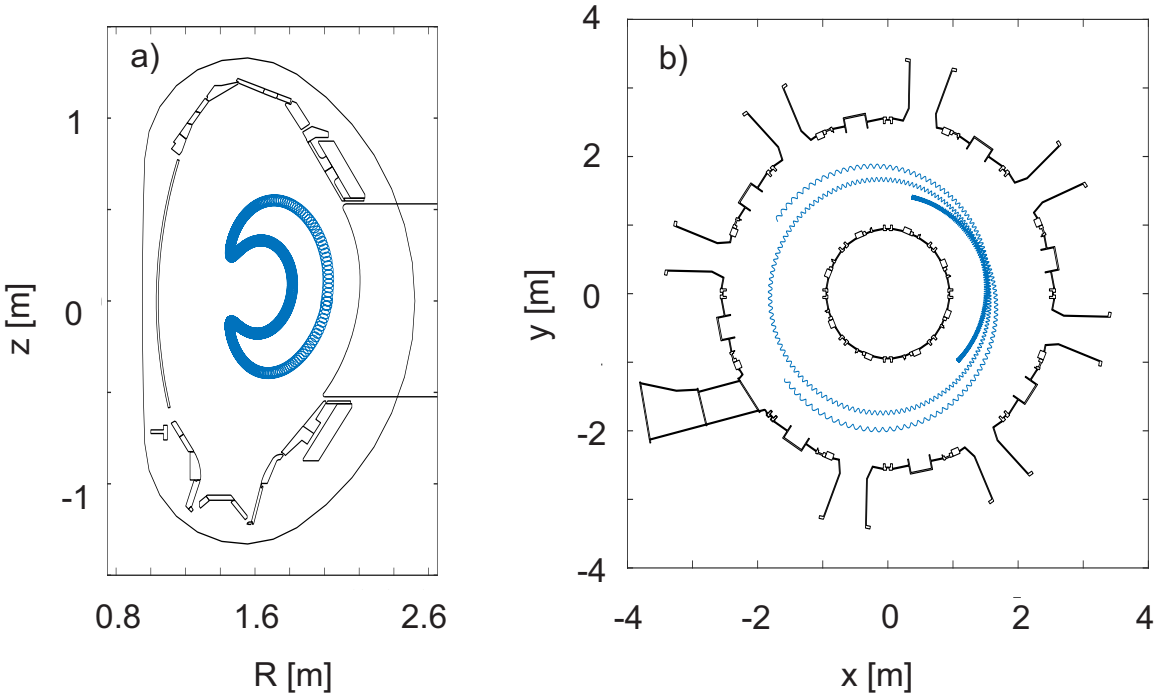

Figure 2.3: Poloidal cross section (a) and toroidal cross section (b) of a trapped trajectory.

2.1.2 Toroidal canonical momentum

If the field is stationary or slowly varying with the magnetic field and there is toroidal symmetry the canonical momentum of the particle does not change along the trajectory of the particle [8]. The expression of the toroidal canonical momentum is,

$$P_\phi = mRv_\phi - Ze\Psi \tag{2.8}$$

where v_ϕ is the toroidal velocity, R is the major radius and Ψ is the poloidal flux.

The variation of the toroidal canonical momentum is related to the radial transport of the ions in the presence of 3D field [6]. The direction of the radial transport is determined by the sign of the variation of the canonical momentum, where a positive variation leads to an inwards transport and a negative variation results into an outward transport.

2.2 Fast-ions

Fast ions are charged particles whose energy is at least one order of magnitude above the thermal energy of the plasma [3]. Fast ions are introduced in the plasma to heat the plasma. The concentration of these ions is around 1% but they could carry half of the

energy of the tokamak plasma. The fast ions can transfer their energy to the plasma when colliding with the thermal particles.

There are three sources of fast ions: Neutral Beam Injection (NBI), Ion Cyclotron Resonance Heating (ICRH) and fusion reactions.

Neutral particles can penetrate the plasma before they are ionized. The NBI consists of charged particles that are accelerated in an accelerator and then neutralized and injected into the plasma. The energy of this beam is high enough to reach the plasma center but if it is too energetic, it can pass through the plasma without being ionized. The particles used are H, D or T ions and they can act as a fuel.

In ICRH heating, radio waves at a harmonic frequency of the ion cyclotron are injected, these ions will be in resonance with the wave. Waves at the cyclotron frequency of the main plasma cannot propagate into the plasma, for this reason a different frequency must be used. Usually minority species (H,$^3He, D$) are heated and tranfer their energy with collisions.

2.3 Magnetic perturbation

The magnetic field in a tokamak is independent of the toroidal coordinate (φ), so this field is axisymmetric. However, the field can be perturbed and this symmetry is lost.

There are three ways in which the magnetic field can be perturbed: toroidal field ripple (due to the finite number of toroidal field coils), magnetized components (ferromagnetic materials are introduced into the tokamak and they become magnetized) and external coils [3].The data is obtained from experiments in ASDEX Upgrade, where there are two sets of eight coils, one installed above the midplane and one below, the geometry of these coils is shown in Figure 2.4. These coils generated the perturbation and are known as B-coils .These perturbations are used to mitigate instabilities such as Edge Localized Modes (ELMs), an instability in the edge of the tokamak that acelerates the erosion of the divertor and the first wall components that expels particles and energy from the plasma, thus leading to the erosion of the divertor and the first wall components [9].

Using external coils [11], a variation of the particle transport is observed. These changes can affect the electron density: the population of electrons in the core or the

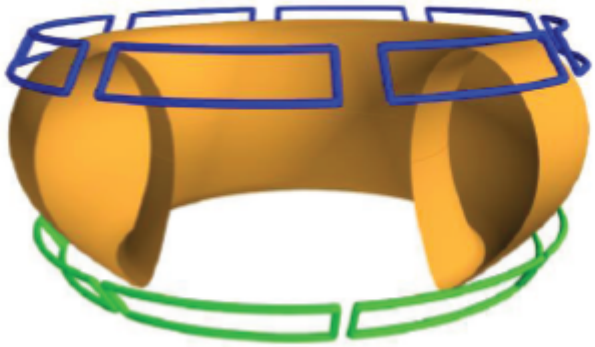

Figure 2.4: Distribution of the Resonant Magnetic Perturbation (RMP) coils along the vessel in green and blue [10].

edge of the tokamak can vary drastically if we apply a magnetic perturbation (MP) [12], [13]. Besides, fast-ions are perfectly confined in axisymmetric fields, but in the presence of MPs these ions can be lost. This is reflected in the variation of the toroidal canonical momentum.

The perturbed part of the magnetic field that is used in these simulations it is shown in Figure 2.5.

Figure 2.5: Perturbation of the magnetic field. (a) Radial component. (b) Azimuthal component. (c) Vertical component. (d) Total perturbation.

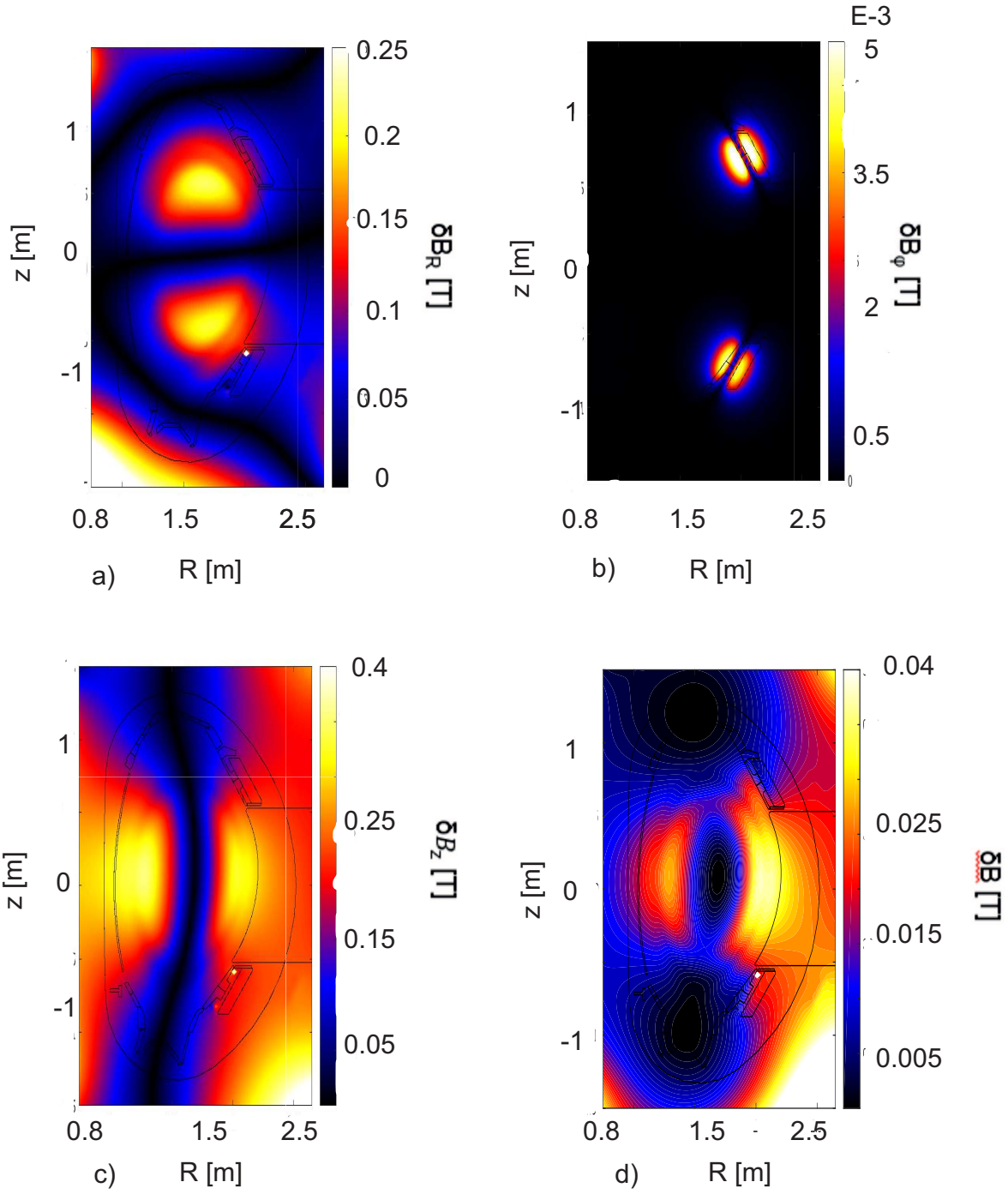

Chapter 3

Description of the ASCOT Code

The ASCOT (Accelerated Simulation of Charged particle Orbits in Tori) code has been developed at Helsinky University of Technology and the Technical Research Center of Finland since the early 1990s [14]. This code can study minority particles in fusion devices using the Monte Carlo method [15].

To calculate the full gyromotion there are two options: a fourth order Runge-Kutta method [16] or a modified leap-frog method. That is defined by,

$$left\vec{v}_{i+1} = \vec{v}_i + \Delta t \frac{e}{m}\left(\vec{E}_i + \frac{\vec{v}_{i+1} + \vec{v}_i}{2} \times \vec{B}_i\right) \tag{3.1}$$

$$\vec{r}_{i+1} = \vec{r}_i + \Delta t \vec{v}_i \tag{3.2}$$

Using the leap-frog method the energy is strictly conserved in absence of an electric field.

A series of input are needed to set up the simulation. The input data must describe the magnetic field, plasma conditions, geometry and test particles.

The magnetic field is a crucial element to obtain the orbits of the particles. In this case, the inputs are 3D magnetic field perturbations combined with the equilibrium magnetic field, however the ripple effect is not included (this effect creates other resonances and in this thesis it is required to isolate the effects of the MP).

In addition, the temperature and densities of the plasma species and the toroidal flow of the plasma. The data is obtained from measurements during experiment (also referred to as shots or discharges in this thesis). In this case, the shots #28061 and #28059 will be used to set up the simulation [5].

The geometry that is required in these simulations is a 2D square wall to reduce the number of particles that hit the wall.

Finally, the distributions of the ions have to be known. In this thesis, the simulations will be initiated scaning in the initial radius, energy or pitch.

The ASCOT Code use a variety of methods to do the calculations. The guiding-centre method follows only the centre of gyration of the particle ignoring the gyrations. This method requires the minimal computational cost in the ASCOT Code, however the information of the gyration is lost during the process. In this thesis, it is used the full orbit method (using the leap-frog integration method) which consists of following the particle through the gyrations. This method is more expensive than the guiding center method but it is required to know the whole trajectories of the particle. Also, there is a hybrid method that combine the guiding center and the full orbit method.

A myriad of data can be collected from a simulation. To set up the simulation, the ASCOT code must know what output it has to collect. Also, the ASCOT code can store all the test particle information each certain time step that the usuary chooses. At the end of the ASCOT simulation, it can be determined location, velocity, pitch angle, energy and simulated time for every test particle. Also, the ASCOT code provides the reasons of the end of the simulations (a particle hits the wall, a particle reaches maximum simulation time...). The ASCOT code allows to replicate the trajectories of the particles under certain experimental conditions.

Chapter 4

Results

4.1 Variation of the toroidal canonical momentum

In this section, the ASCOT code has followed 19881 particles during a maximum time of 5 10^{-4} s. The simulation has scanned initial radius, pitch angle and energy and calculated the toroidal canonical momentum. The initial vertical coordinate is zero and the initial azimuthal coordinate is 3.806 rad in all the particles.

If the magnetic field is axisymmetric (no external magnetic perturbation is applied) the toroidal canonical momentum of a particle is conserved. This is showed in Figure 4.1. where the variation of the toroidal canonical momentum is plotted as a function of the energy, the pitch angle and the radius. In plot (a) the code varys the initial energy and radius while the initial pitch angle remains constant, in plot (b), the code varys the initial pitch angle (in this section, the pitch is redefined as $v_{\|}/v$) and radius while the energy remains constant along the figure.

External magnetic perturbations generated by the B-coils [5] were applied during the discharges #28059 and #28061. The evolution of the B-coils current is shown in Figure 4.2.

Analysis of the evolution of the toroidal canonical momentum in the discharge #28061 while MP are applied ($t = 4.66s$) shown a variation of the toroidal canonical momentum with respect to Figure 4.1.

In Figure 4.3 (a), a series of resonances from the particles (a resonance is produced when the toroidal canonical momentum varys [17]) are observed. These resonances are related to a radial transport. To make easier the analysis, the plot is split up into four

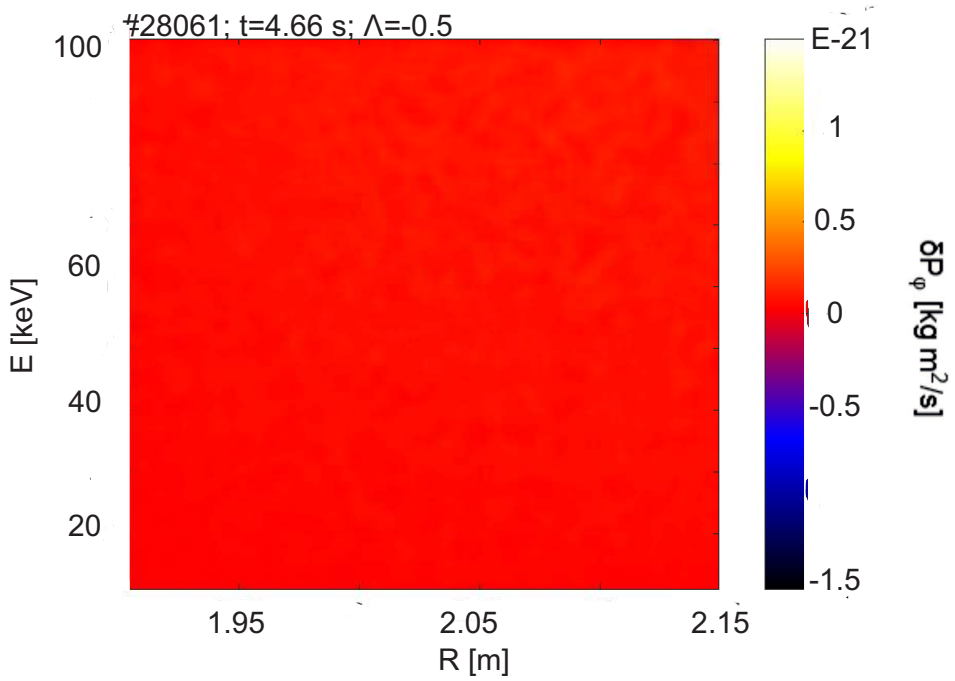

(a) Variation of the canonical momentum as a function of the particle initial energy and radius.

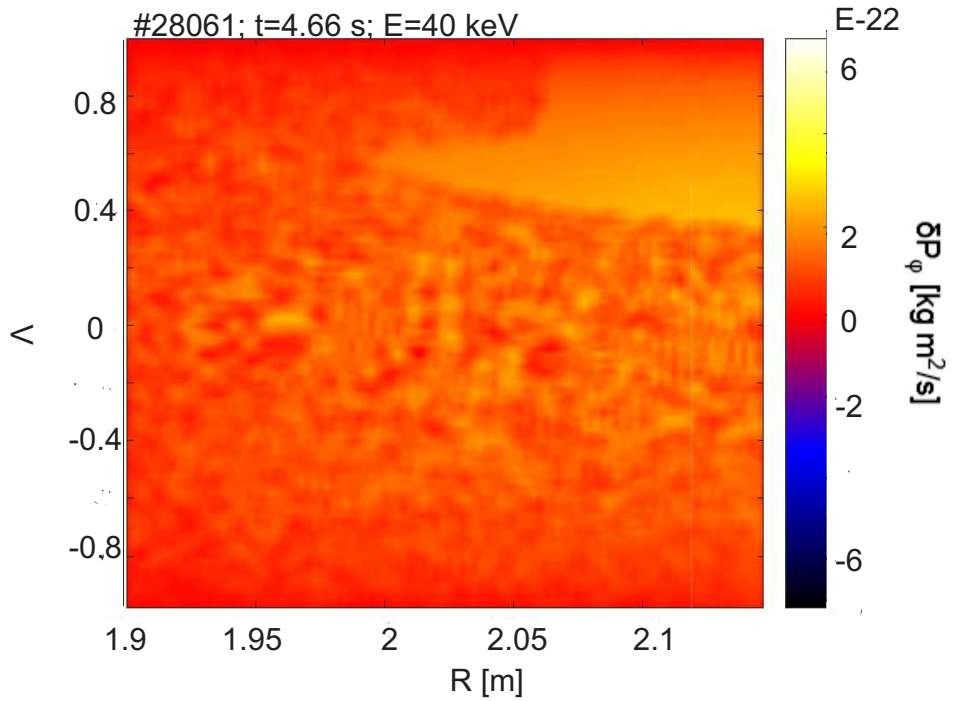

(b) Variation of the canonical momentum as a function of the particle initial pitch angle and radius.

Figure 4.1: Variation of the toroidal canonical momentum without the perturbation. Shot #28061.

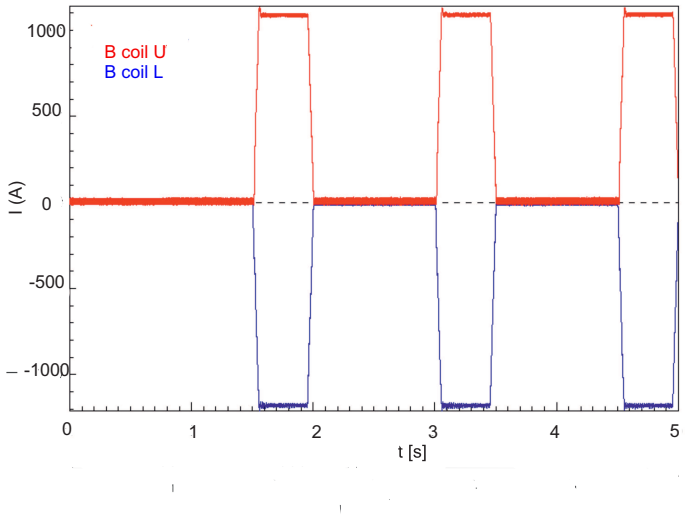

(a) Shot #28061

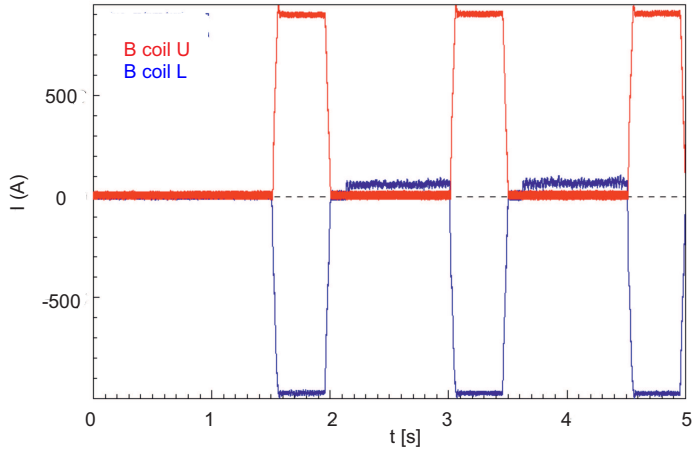

(b) Shot #28059

Figure 4.2: Temporal evolution of the B-coils current.

zones (marked with I-IV in Figure 4.3 (a)) . In each one of these regions the variation of the toroidal canonical momentum changes its sign.

The plot (b) of the Figure 4.3. shows the variation of the toroidal canonical momentum in function of the initial pitch angle and radius. The ressonance that it is seen before the separatrix match with the trapped-passing boundary. After the separatrix, new resonances appear at high pitch angles.

In the first zone of the Figure 4.3 (a), before we cross the trapped-passing boundary , all the trajectories are passing and the toroidal canonical momentum does not vary. Resonances begin to appear in the following zones and the particles has a desviation of

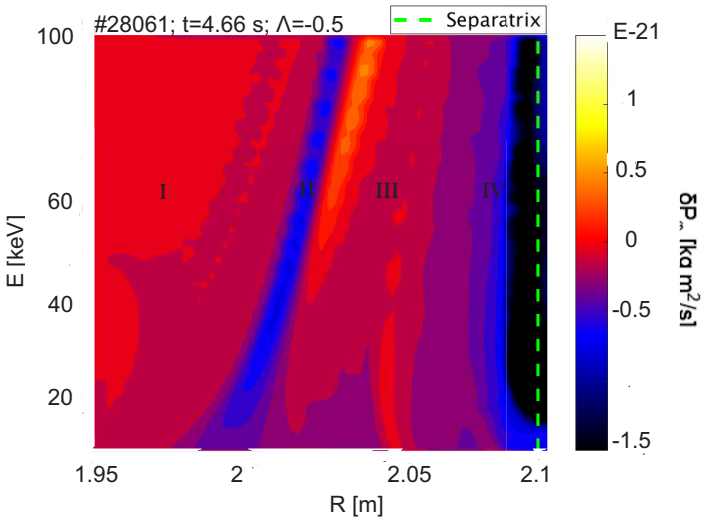

(a) Variation of the canonical momentum as a function of the particle initial energy and radius.

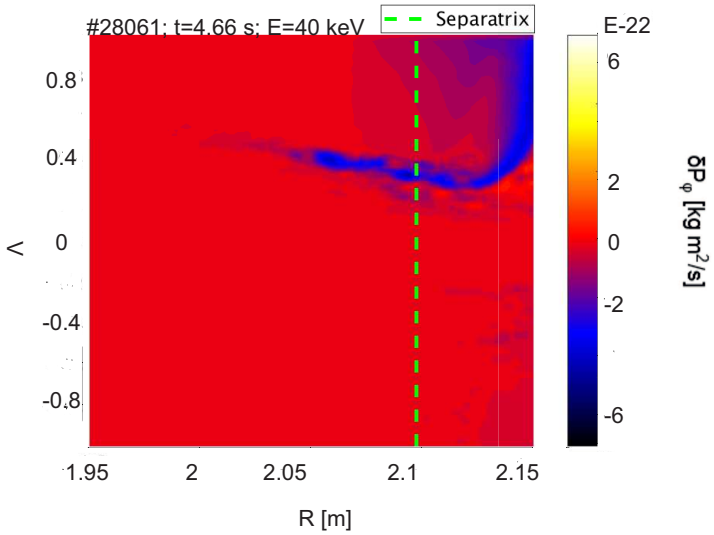

(b) Variation of the canonical momentum as a function of the particle initial pitch angle and radius.

Figure 4.3: Variation of the canonical momentum. Shot #28061 at 4.66 s.

the behaviour that it is shown in Figure 4.1. The following figures analyze and compare concretes trajectories in each regions.

In Figure 4.4, it is shown the temporal evolution of the toroidal canonical momentum and trajectories of two particles that are originated in the same coordinates, but its equilibrium is different. The blue line is the temporal evolution of the toroidal canonical momentum and trajectory of a particle whose magnetic field has been perturbed and the red lines represent a particle whose equilibrium is axisymmetric.

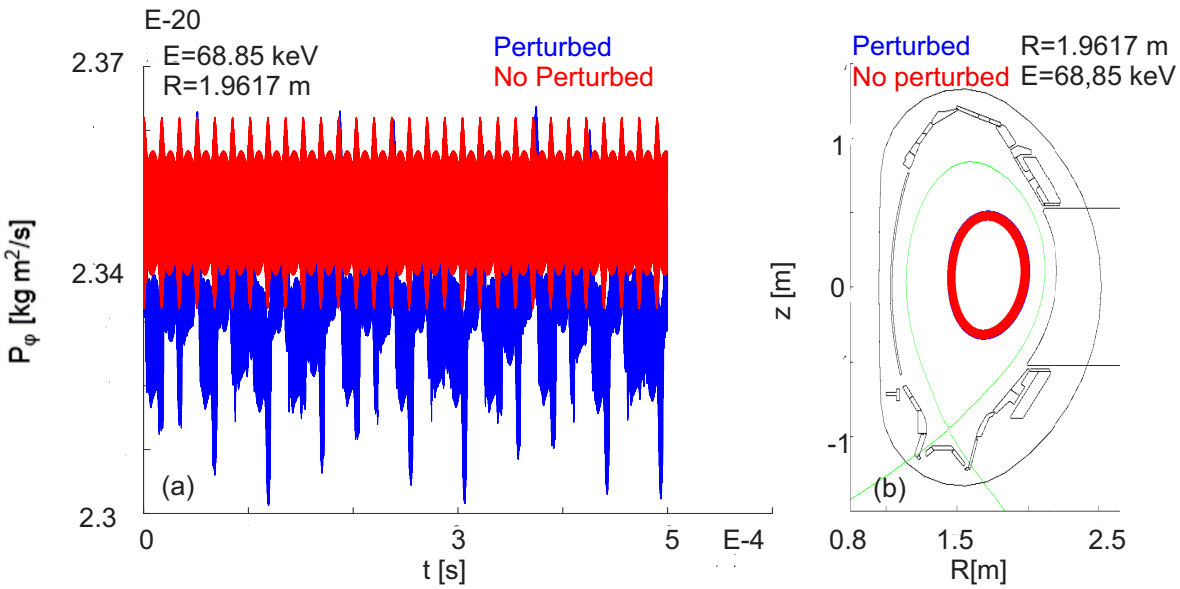

Figure 4.4: Temporal evolution of the toroidal canonical momentum (a) and trajectory in the poloidal cross section (b) for a particle in axisymmetric equilibrium (red) and a particle with MP (blue).

The next region (Zone II) crosses the trapped-passing boundary which contains multiple resonances. The change of the canonical momentum is usually maximum (minimum) in this region. The trapped-pasing boundary would be between the Zone I and II when the toroidal canonical momentum changes drastically its sign.

In the next region (Zone III), it is shown that the trajectories are trapped (Figure 4.5) and the variation of the canonical momentum is significant. The variation of the transport is related to the magnetic perturbation (Figure 2.4). In Figure 4.5, the transport increases when the particles are in resonance with the perturbation.

Then, in the next region (Zone IV) we obtain the Figure 4.6 and a point when the toroidal canonical momentum decreases more than the previous cases. The transport has the opposite direction that the previous case (it is outward instead of inward). This zone is the closest to the separatrix.

In Annex A and B are shown the change of the canonical momentum with other time points for discharge #28061 while the magnetic perturbation is still applied. The equilibrium used in Annex A and B are at time points 3.25s and 1.75s, respectively.

Figure 4.3 and the plots shown in annexs A and B are very similar. The field that is applied in these cases is the same so it is expected that there is no variation in the results. This is confirmed by obtaining the same variation of the toroidal canonical momentum at

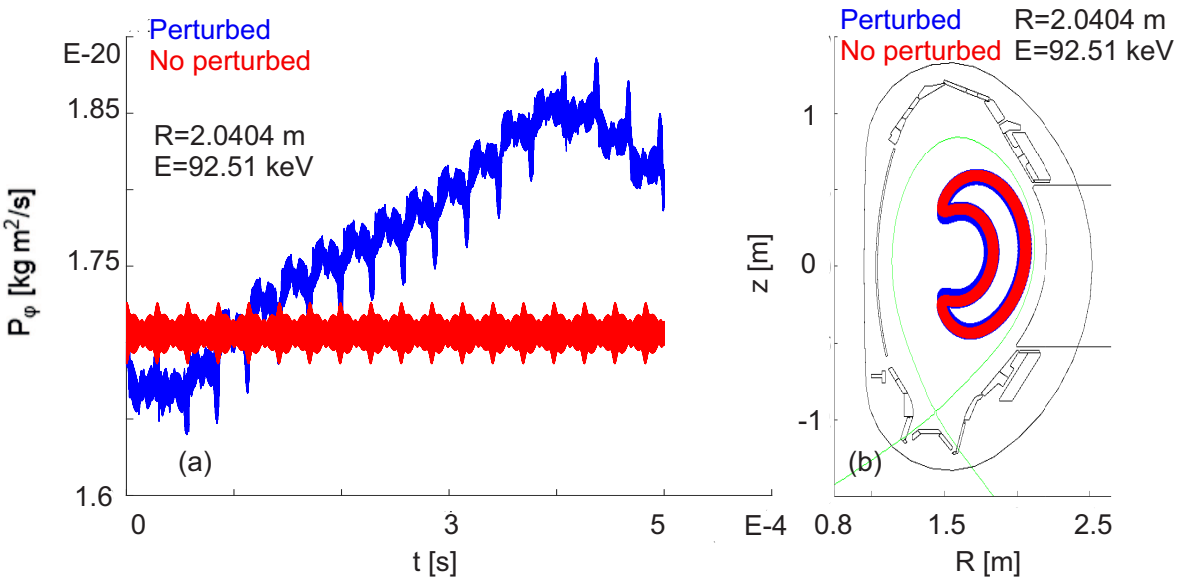

Figure 4.5: Temporal evolution of the toroidal canonical momentum (a) and trajectory in the poloidal cross section (b) for a particle in axisymmetric equilibrium (red) and a particle with MP (blue).

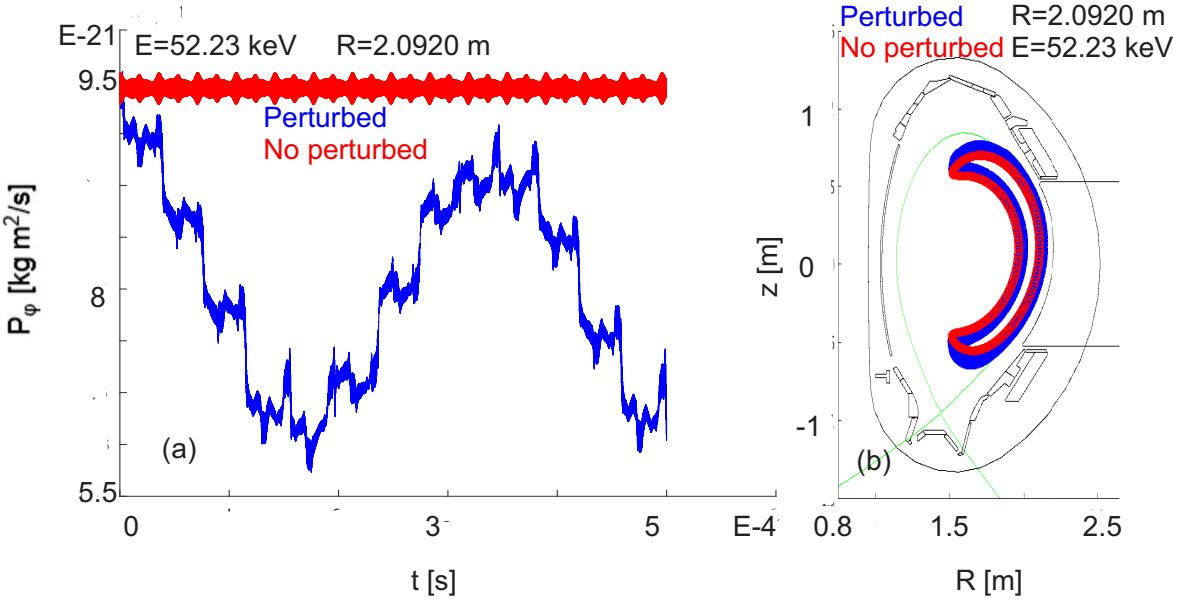

Figure 4.6: Temporal evolution of the toroidal canonical momentum (a) and trajectory in the poloidal cross section (b) for a particle in axisymmetric equilibrium (red) and a particle with MP (blue).

the different time points for a particle of a given energy. Figure 4.7 represents variation of the toroidal canonical momentum in function of the initial radius at a given time point and energy, there is no variation in the behaviour of the three time points.

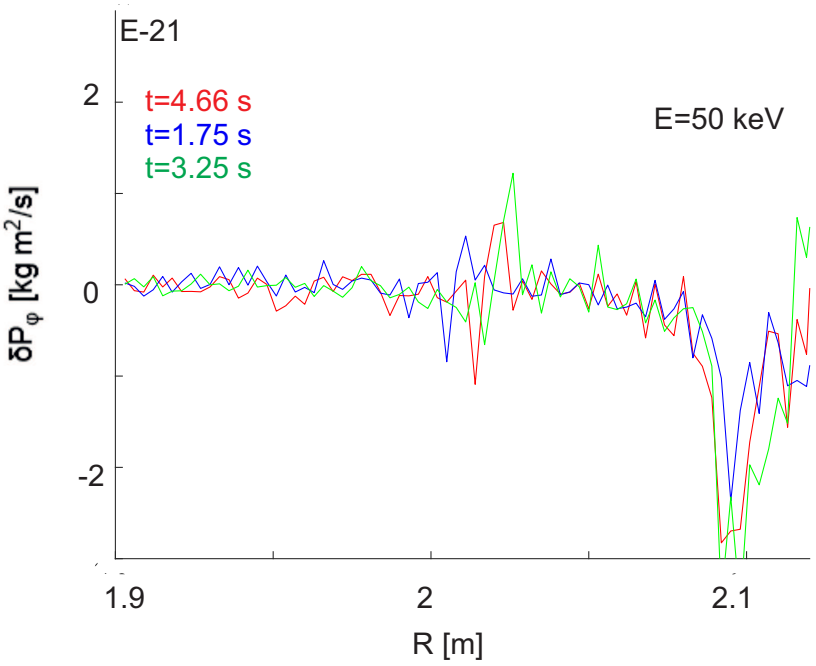

Figure 4.7: Variation of the toroidal as a function of the radius at 50 keV at different times.

Besides that, the magnetic perturbation and the equilibrium of the shot #28059 are different from the previous case, the intensity of the magnetic field in the shot #28059 is lower than the magnetic field in the shot #28061 [5] and the MPs applied are differents (Figure 4.2.). For this reason, the change of the toroidal canonical momentum will be different. The variation of the toroidal canonical momentum of the shot #28059 is shown in Annex C. The trapped-passing boundary is further away from the separatrix compared to the previous case and we can see five different zones instead of four zones. In the fifth zone the toroidal canonical momentum increases, in this zone the transport will be an inward instead of an outward transport. The variation of the toroidal canonical momentum in function of the initial pitch and the radius is similar to the previous cases.

The variation of the toroidal canonical momentum of a particle of a given energy for shots #28061 and #28059 (Figure 4.8) presents a different behaviour (for $R > 2.05m$ there is a gain/loss of the toroidal canonical momentum for discharges #28059 and #28061, respectivelly).

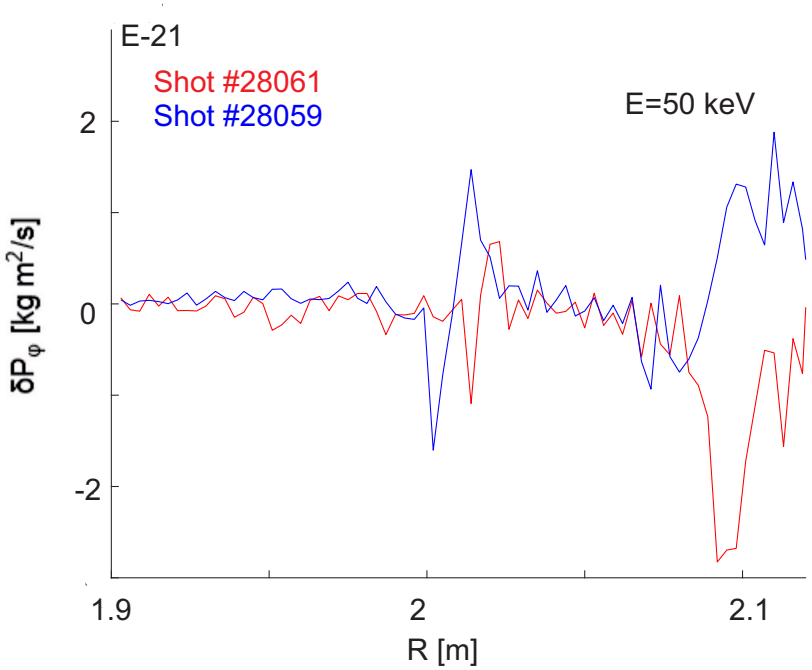

Figure 4.8: Variation of the toroidal as a function of the radius at 50 keV at different shots.

4.2 Impact of the orbits topology in the correlation maps

Once we see the effects of the magnetic perturbations in the canonical momentum we can compare the correlations that are obtained in [5] with the position of the trapped-passing boundary.

In this section, the ASCOT code has followed 59643 particles during a maximum time of 5 10^{-4} s. The simulation has scanned initial pitch angle and energy (Eq. 2.2). The initial azimuthal and the vertical coordinates are the same that the previous section.The trapped-passing boundary has been obtained analyzing the temporal evolution of the sign of the pitch (in trapped trajectories the pitch changes its sign, but in passing trajectories its sign remains constant).

Figure 4.9 shows a superposition between the results obtained in the simulations and the results from [5]. Figure 4.9 also shows that the changes in the correlation between fast-ions losses and impurity toroidal rotation match with the trapped-passing boundary.

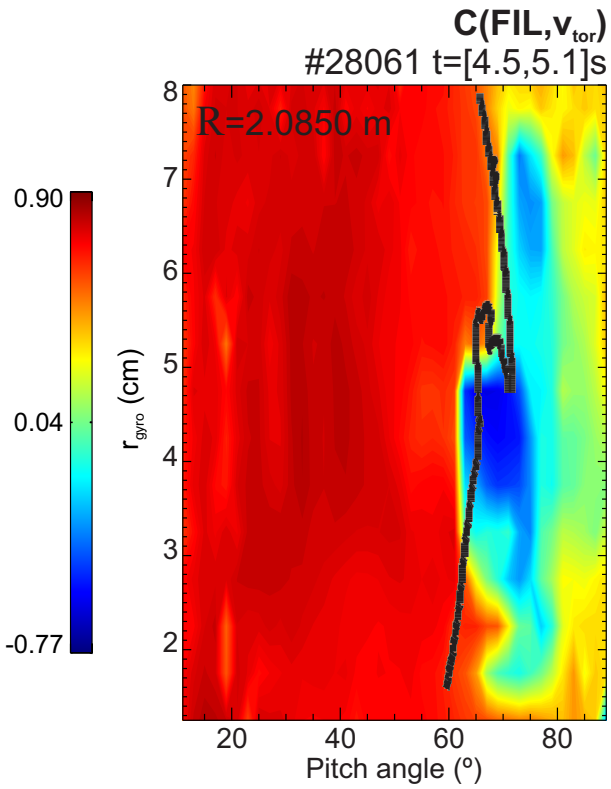

Figure 4.9: Comparison of correlation fast ions losses and impurity toroidal rotation with trapped-passing boundary (black line).

Chapter 5

Conclusions

The ASCOT code was used to simulate the impact of externally applied magnetic perturbations on the plasma. The simulation results are in agreement with our expectations [6],[5] in terms of the behaviour of the particles and their dependecies with the initial condition and the equilibrium.

The variation of the canonical momentum gives us information about the transport of the particles and the type of trajectories found in each region. When the variation of the canonical momentum is larger, an accentuated drift is produced and differents regions appear where the type of transport changes. The toroidal canonical momentum depends on the perturbation that is applied, the axisymmetric equilibrium, the initial radius, energy or pitch that particles have. These parameters can be studied to control the transport of the fast-ions.

Besides that, the results of this thesis have been compared with the results of [5] and the correlations of the toroidal rotation and fast-ion transport agree with the trapped-passing boundary and it is confirmed that there is a relation between the correlations studied in the previous thesis the topology of the orbits.

These results shed more light of the effect of the 3D applied magnetic field. In this thesis, we confirmed correlation and dependencies with the trajectories of the particles. This knowledge shed more ligth of the of the 3D applied magnetic field and allow to predict the consequences of the magnetic perturbations.

Acknowledgements

First, I want to thanks the supervisors of this thesis Dr. Eleonora Viezzer and Dr. Manolo García Muñoz for the chance to work in this subject.

I want to thank Lucía for her help with the first programs in the ASCOT code and the reviews of the figures of this thesis.

I also want to thank Pilar, I will never be able to complete this work without her help. Thanks for my first steps in ASCOT, thanks for the first simulations, thanks for the all the corrections and advices. I appreciate your help.

Finally, all my classmates in all these years of studying, learning and laughing deserve to be mentioned, without them I will not be here today.

Bibliography

[1] J. Wesson. *Tokamaks*. 3^{rd} edition, ISBN 0 19 8509227, Oxford University Press, Oxford, 2004.

[2] Cross section of fusion reaction. URL `https://commons.wikimedia.org/wiki/File:Fusion_rxnrate.svg`, 2014. [Online; accessed 26-November-2018].

[3] T. Koskela. *Monte Carlo simulation of fast ion losses in ITER in the presence of static 3D magnetic perturbations*. ISBN 978-952-60-6004-0, Aalto University, 2014.

[4] Tokamak schematics. URL `https://commons.wikimedia.org/wiki/File:Torusdrift_and_twisted_magnetic_field.png`, 2013. [Online; accessed 26-November-2018].

[5] P. Cano Megías. *Impact of externally applied 3D fields on plasma rotation and correlation to particle losses*. Master thesis at Univesidad de Sevilla, 2017.

[6] L Sanchis *et al. Plasma Phys. and Control. Fusion*, 61:014038, 2019.

[7] Drift. URL `https://ocw.mit.edu/courses/nuclear-engineering/22-611j-introduction-to-plasma-physics-i-fall-2003/lecture-notes/chap2.pdf`, 2003. [Online; accessed 26-November-2018].

[8] A. Salmi. *Fast ions and momentum transport in JET tokamak plasmas*. 2012.

[9] Edge located mode. URL `https://www.iter.org/newsline/259/1509`, 2013. [Online; accessed 26-November-2018].

[10] Y. Liu *et al. Plasma Phys. and Control. Fusion*, 58:114005, 2016.

[11] M. Garcia-Munoz *et al. Plasma Phys. and Control. Fusion*, 55:4014–, 2013.

[12] W. A. Suttrop *et al. Plys. Rev. and Lett.*, 106:225004, 2011.

[13] M. Garcia-Munoz *et al. Phys. Rev. Lett.*, 92:235003, 2004.

[14] E. Hirvijoki*et al. Computer Physics Communications*, 185:1310 – 1321, 2014.

[15] Monte carlo method. URL `http://www.palisade.com/risk/monte_carlo_simulation.asp`. [Online; accessed 26-November-2018].

[16] Fourth order runge-kutta method. URL `http://www.math.ubc.ca/~israel/m215/runge/runge.html`. [Online; accessed 26-November-2018].

[17] F. Nabais *et al. Nuclear Fusion*, 52:083021, 2012.

Annex A: Variation of the canonical momentum. Shot #28061 at 3.25 s.

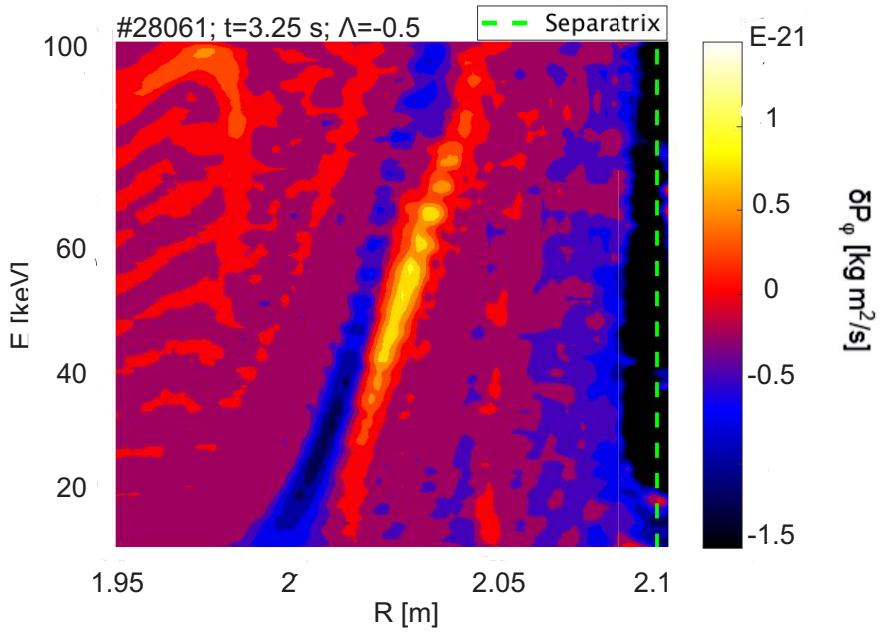

(a) Variation of the canonical momentum as a function of the particle initial energy and radius

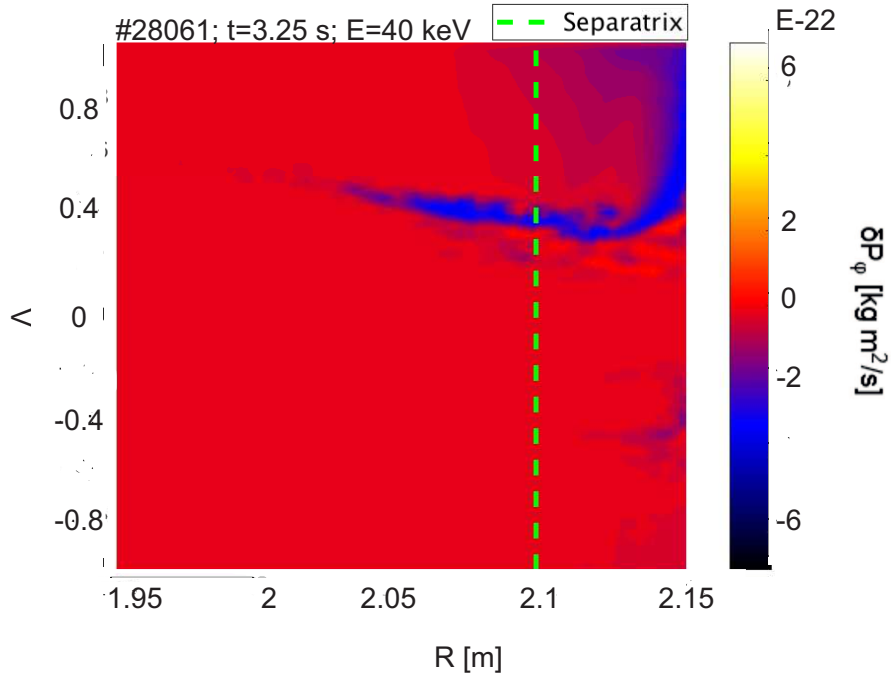

(b) Variation of the canonical momentum as a function of the particle initial pitch angle and radius.

Figure A.1. Variation of the canonical momentum. Shot #28061 at 3.25 s

Annex B: Variation of the canonical momentum. Shot #28061 at 1.75 s.

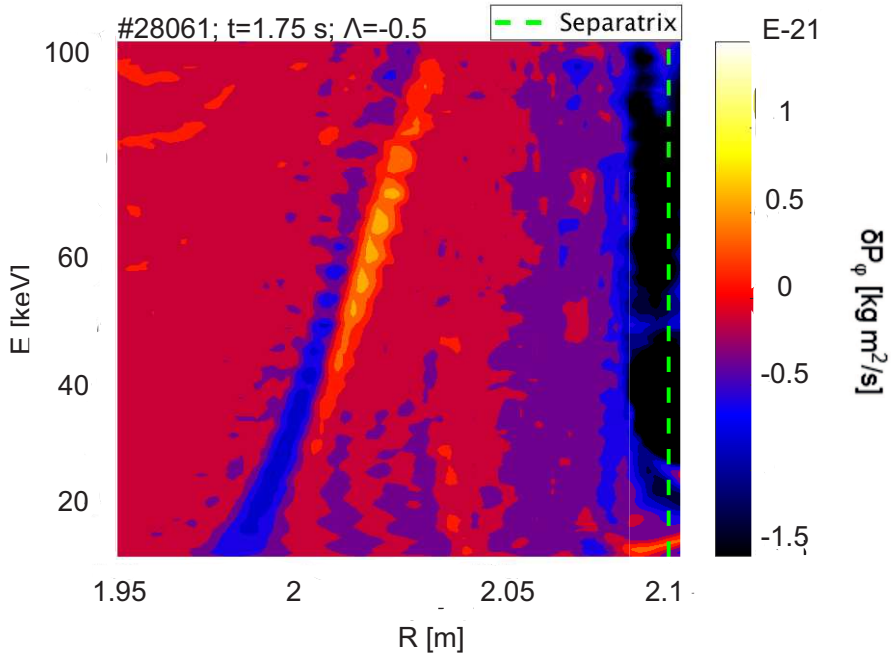

(a) Variation of the canonical momentum as a function of the particle initial energy and radius

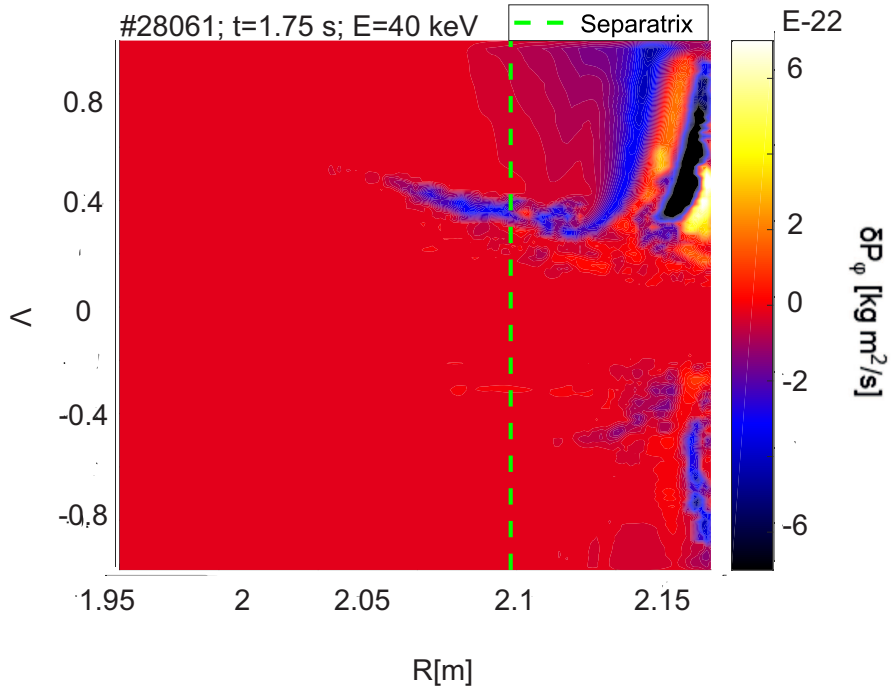

(b) Variation of the canonical momentum as a function of the particle initial pitch angle and radius.

Figure B.1. Variation of the canonical momentum. Shot #28061 at 1.75 s.

Annex C: Variation of the canonical momentum. Shot #28059 at 4.75 s.

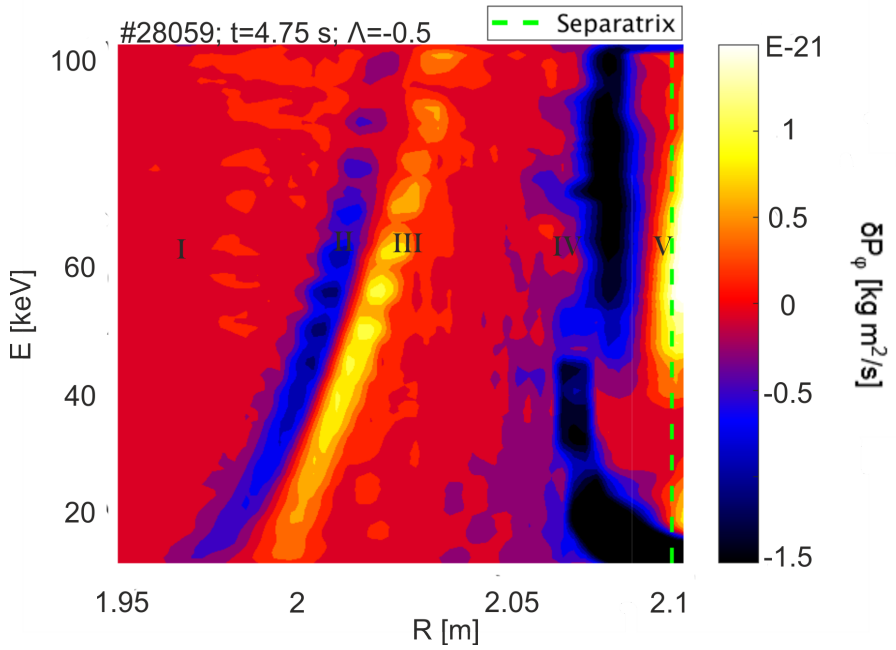

(a) Variation of the canonical momentum as a function of the particle initial energy and radius

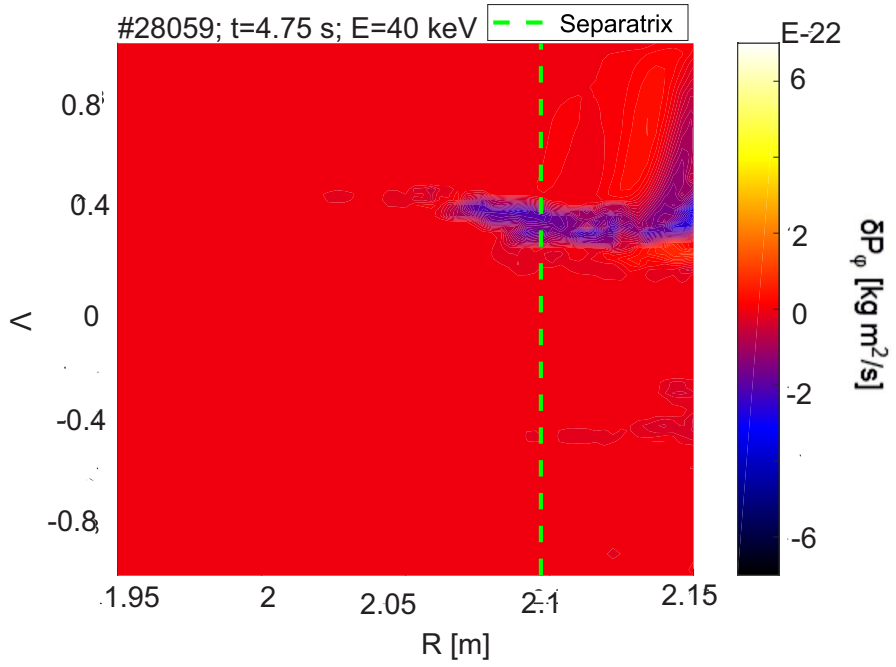

(b) Variation of the canonical momentum as a function of the particle initial pitch angle and radius.

Figure C.1. Variation of the canonical momentum. Shot #28059 at 4.75 s.